

A pulsed high-voltage decelerator system to deliver low-energy antiprotons

The GBAR Collaboration

(author list appended)

Abstract

The GBAR (Gravitational Behavior of Antihydrogen at Rest) experiment at CERN requires efficient deceleration of 100 keV antiprotons provided by the new ELENA synchrotron ring to synthesize antihydrogen. This is accomplished using electrostatic deceleration optics and a drift tube that is designed to switch from -99 kV to ground when the antiproton bunch is inside - essentially a charged-particle “elevator” - producing a 1 keV pulse. We describe the simulation, design, construction and successful testing of the decelerator device at -92 kV on-line with ELENA.

Keywords: Antihydrogen, General Relativity, Charged-particle optics, ion-optic simulations

1. Introduction

2 The GBAR (Gravitational Behavior of Antihydrogen at Rest) experiment
3 [1] at CERN aims at testing the Weak Equivalence Principle (WEP) of Gen-
4 eral Relativity by measuring the free fall of antihydrogen ($\bar{\text{H}}$) in the Earth’s
5 gravitational field. The WEP has been stringently tested in different regimes
6 but never using antimatter, which may fall with a different acceleration than

7 for matter. Such an experiment requires extremely well-defined initial con-
8 ditions, with near-zero initial velocity. While this goal is likewise pursued
9 by the CERN experiments ALPHA [2] and AEGIS [3], GBAR will attempt a
10 unique approach by synthesizing antihydrogen ions ($\bar{\text{H}}^+$) that can be sympa-
11 thetically cooled by coupling to a laser-cooled trapped-Be-ion crystal [4, 5, 6],
12 reaching velocities of about 1 m/s (60 μK).

13 GBAR will fabricate antihydrogen using the electron-positron atomic sys-
14 tem, positronium (Ps) created by directing positrons onto a mesoporous sil-
15 ica target [7]. Antiprotons sent through the Ps cloud undergo two successive
16 charge-exchange reactions, forming $\bar{\text{H}}$ and $\bar{\text{H}}^+$. Producing $\bar{\text{H}}^+$ requires a
17 higher positron flux than achievable with a radioactive source. Therefore,
18 the positrons required to form a Ps cloud of sufficient density are generated
19 using a 9 MeV electron linear accelerator [8], cooled in a buffer-gas magnetic
20 trap and then accumulated in a 5 T Penning-Malmberg trap [9] before being
21 directed onto the target.

22 The Ps reaction for the formation of antihydrogen was proposed by Hum-
23 berston et al. [10] and first cross-section measurements were performed by
24 Merrison et al. [11] at energies down to 11.3 keV. The predictions of various
25 atomic-physics models reported in [11] did not agree on the most favorable
26 energy but more recent calculations [12, 13] predict that even lower antipro-
27 ton energies would lead to higher cross sections, hence better $\bar{\text{H}}$ and $\bar{\text{H}}^+$
28 production rates. Refined calculations are in progress to probe this impor-
29 tant question [14].

30 The $\bar{\text{H}}^+$ ions for GBAR will be fabricated using antiprotons delivered
31 by the CERN AD-ELENA facility [15]. The ELENA synchrotron heralds a

32 new era of antiproton and antimatter physics. Its deceleration of antiprotons
33 from 5.3 MeV to 100 keV bridges an important gap to achieve more efficient
34 antihydrogen fabrication and storage at sub-Kelvin temperatures.

35 The first capture of antiprotons into a Penning trap was performed by
36 Gabrielse et al. [16] using a beryllium energy-degrader foil for a 150 ns
37 burst of 10^8 antiprotons delivered at 21.3 MeV by CERN's LEAR facility.
38 CERN's AD facility later provided pulses of 3×10^7 antiprotons at 5.3
39 MeV, allowing the use of thinner foils to achieve rates of about 20000/shot
40 [17]. The ASACUSA experiment further reduced this energy to below 100
41 keV, using a radiofrequency quadrupole linear accelerator operated in reverse
42 mode [18, 19, 20]. The lower incident beam energy allowed the use of foils
43 that were 800 times thinner than in [16] and improved the number of trapped
44 antiprotons by a factor of 50 [19].

45 Using electrostatic deceleration would ideally avoid all losses associated
46 with the use of foils. ELENA now allows using electrostatic retardation
47 and fast switching to reach the energy regime favorable for antihydrogen
48 formation by charge exchange.

49 This article describes a novel multi-electrode deceleration system that
50 creates a 100 keV particle "elevator". This is accomplished using electrostatic
51 retardation optics and a drift tube that is switched from -99 kV to ground
52 during the short time that the antiproton bunch is inside. Further optics
53 focus the low-energy beam into the Ps reaction chamber. Simulations for
54 the optimization of the potential values are described, as well as the design,
55 construction and preliminary testing of the decelerator device down to -92 kV
56 using H^- and antiprotons from ELENA during its commissioning period.

57 2. Design and construction of the decelerator

58 The concept of the decelerator and results from first tests with the pro-
59 totype have been described in [21, 22, 23]. The principle is to use a static
60 electric field to slow the charged antiprotons into a drift tube, within which
61 there are ideally no potential gradients. Once the antiproton pulse is inside
62 the field-free region, the voltage applied to the tube is switched to ground. If
63 the switching is fast enough, there will be no voltage gradient at the exit of
64 the tube when the antiprotons arrive, so they continue at their decelerated
65 kinetic energy. Of course the use of drift tubes for changing the energy of
66 particle beams is not new. Drift tubes form the heart of linear accelerators
67 using AC voltages, however their use as particle elevators is less common.
68 The so-called pulsed drift tube is used at many nuclear physics facilities
69 where ion species are transported with energies of 30-60 keV and must be
70 slowed to a few eV to be confined in a trap. The deceleration of the ion bunch
71 causes the beam emittance to blow up so that the ions must be cooled to be
72 trapped. The technique was largely developed by the ISOLTRAP experiment
73 at CERN's ISOLDE facility, in conjunction with a device for accumulating
74 ISOLDE beams [24]. In this scheme, the beam is decelerated into a linear
75 radiofrequency trap filled with buffer gas, which cools the large emittance
76 of the decelerated beam to essentially a point-like source. The drift tube
77 is mounted directly downstream of the trap. This scheme is now used by
78 several on-line trap facilities.

79 The main difference with the decelerator presented here is that since an-
80 tiprotons would annihilate with the buffer gas atoms the deceleration process
81 must include optics to keep the larger emittance within the drift-tube elec-

82 trode and limit divergence in the region of potential gradients.

83 A deceleration system for ion beams that did not incorporate a gas-filled
84 cooler buncher was designed for the WITCH experiment at ISOLDE by Coeck
85 et al. [25]. The beam was cooled in a gas-filled Penning trap a few meters
86 upstream and reaccelerated. The drift tube was almost 700 mm long and
87 used an intermediate deceleration electrode to limit the beam divergence,
88 decelerating 43 % of the incident 30 keV beam with 24 kV on the drift
89 tube. A similar scheme for 30 keV ions was developed for the TRIGATRAP
90 experiment in Mainz [26].

91 Decelerating 100 keV ELENA beams requires a substantial scaling from
92 the 30 kV systems mentioned above. ELENA was designed to provide
93 antiproton bunches of 300 ns duration (defined as four times rms value of
94 75 ns that includes 95% of an approximately Gaussian distribution), 0.25%
95 momentum spread and about 4π mm mrad transverse emittance [15]. When
96 the 100 keV beam is decelerated to 1 keV, the transverse emittance increases
97 to 40π mm mrad and the 1.3 m pulse length is reduced to about 150 mm. We
98 consequently chose a drift-tube length of 400 mm to allow enough time for
99 switching within a field-free region.

100 The first consequence of decelerating the beam is a large divergence, which
101 will cause huge losses inside a long drift tube. It is also critical to preserve
102 good focusing properties of the beam by avoiding aberrations during the de-
103 celeration. This requires keeping the beam as parallel as possible, especially
104 where the field gradient is large, and necessitates extra degrees of freedom
105 for the optics. The work of C. Smorra for the TRIGATRAP drift tube [27]
106 gives an excellent illustration.

107 Simulations were performed using the ion-optics program SIMION[®], start-
108 ing with three electrodes (in the familiar einzel lens geometry). The deceler-
109 ated beam retained a rather large diameter that was considered too dangerous
110 for good focusing (the GBAR experiment requires directing the decelerated
111 beam into a 1 mm diameter cavity). This solution also led to large variations
112 in divergence for small changes in deceleration voltage. Therefore a second
113 triplet geometry was introduced to provide more flexibility in shaping the
114 beam and reducing the diameter. We also reasoned that any of the addi-
115 tional lenses could always be set to zero if they were not necessary. It is
116 interesting to note that the work of Coeck et al. [25] concluded with the
117 proposition of including extra electrodes to improve their decelerator design.

118

119 An example of a SIMION[®] trajectory calculation is shown in Fig. 1,
120 which refocuses the decelerated beam near the entrance of the drift tube.
121 The antiproton beam arrives from the left at 100 keV and exits the drift
122 tube with only 1 keV since the voltage on the tube is switched to ground
123 while the ion bunch is inside. Despite different combinations of the different
124 voltages, the output beam is relatively divergent so that an additional Einzel
125 lens is required downstream.

126 In addition to steering electrodes, the ELENA LNE50 extraction beamline
127 includes two quadrupole doublets, which can produce a convergent, parallel,
128 or diverging beam at the decelerator entrance. The trajectories shown in
129 Fig. 1 were calculated with the parallel ELENA beam, which was found to
130 be the most favorable. The beam diameter is 18 mm.

131 A drawing of the decelerator system vacuum chambers and electrodes is

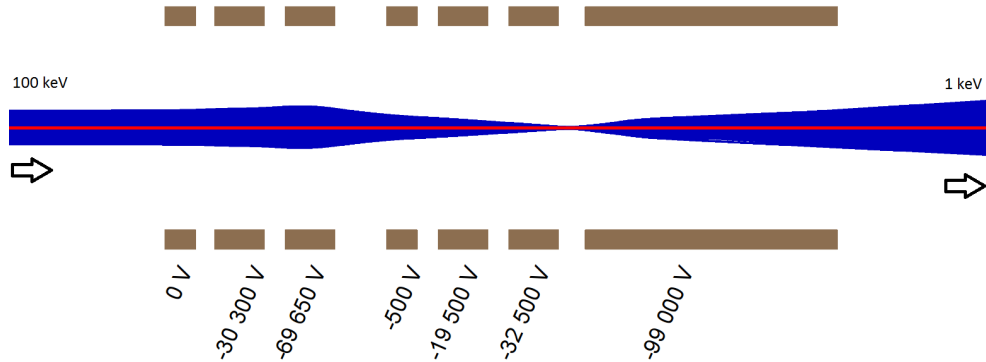


Figure 1: Antiproton trajectories in the decelerator (travelling left to right), calculated by the SIMION[®] program for the potentials indicated on the six (100 mm diameter) electrodes that slow and focus the beam. The potential on the drift tube (-99 kV) is switched to ground when the antiproton pulse is inside. Input beam parameters are the nominal ELENA values given in the text. The output beam energy is 1 keV.

132 shown in Fig. 2. The dimensions were chosen so that the electrodes are large
 133 enough (100 mm diameter) to accept the beam without difficulty but far
 134 enough from the DN250CF chamber walls to avoid sparking. The deceleration
 135 electrodes are arranged as triplets, insulated via MACOR[®] (Machinable
 136 glass ceramic by Corning) to a support frame in the chamber. The overall
 137 length is 1225 mm with an additional 225 mm chamber housing a low-energy
 138 Einzel-lens assembly to focus the decelerated beam into the GBAR reaction
 139 chamber downstream.

140 From the simulations shown in Fig.1 relatively high voltages are required
 141 on the decelerator electrodes, making the geometry and connections non-
 142 trivial. It is critical not to place wires near the chamber walls and to avoid
 143 any sharp edges. Photographs of the second electrode set and the pulsed drift
 144 tube are shown in Fig. 3. The drift tube, required to hold -100 kV, is sup-

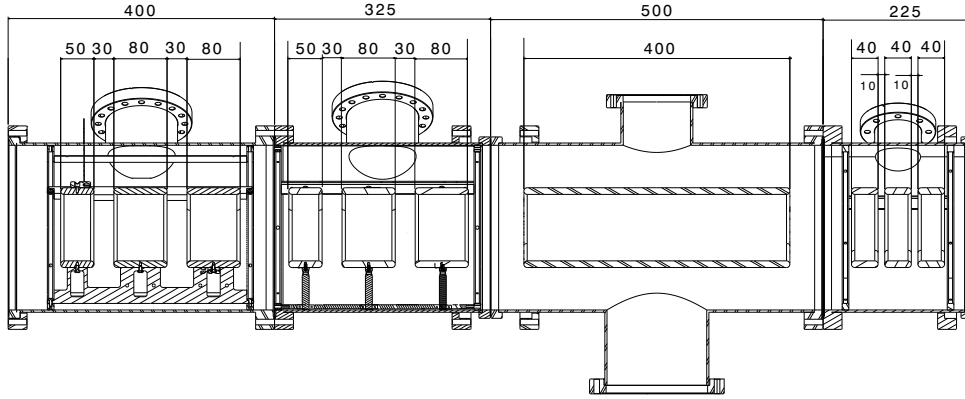


Figure 2: Computer-aided design drawing of the DN250CF vacuum chambers with electrode lengths indicated (all diameters are 100 mm).

145 ported by a specially designed “cradle” (Fig. 3, right) made from MACOR[®]
 146 to avoid the presence of any metallic surfaces. The connection was made
 147 using a metal rod, screwed perpendicularly into the drift tube itself.

148 Connecting the power supplies to the high-voltage vacuum feedthroughs
 149 required embedding the wire inside a rounded bushing, since the threads on
 150 the feedthroughs create corona discharge in air if not covered. Because of
 151 the exceptionally high voltage on the drift tube, the air-side feedthrough was
 152 connected inside a hollow (brass) metal ball. Connecting the drift tube to
 153 the high-voltage switch (150 kV Behlke model HTS 1501-20-LC2) was done
 154 through high-voltage resistors, each of which was connected using metallic
 155 balls to avoid edges. A photograph of the switching circuit is shown in Fig. 4
 156 along with the schematic diagram. The various elements are clad with teflon
 157 for increased protection against discharges (see inset of Fig. 4) and enclosed
 158 in a copper box for electromagnetic shielding.

159 Three high-voltage, non-inductive (Nicrom Electronics, series 500) resis-

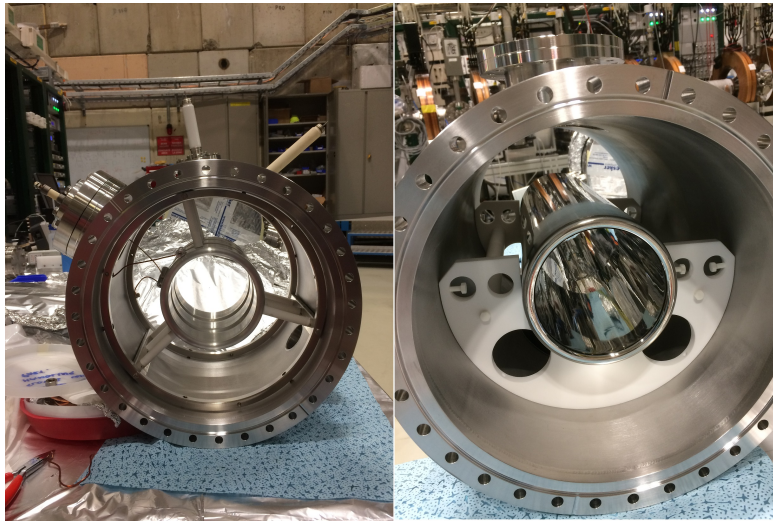


Figure 3: Photographs of: (left) the second set of decelerating electrodes, mounted in their 250CF vacuum chamber on MACOR[®] stand-offs; (right) the pulsed drift tube, machined from stainless steel, mounted on a MACOR[®] “cradle” for stability and insulation.

160 tors are visible in Fig. 4. A $1\text{ G}\Omega$ resistor (right) avoids short circuiting the
161 power supply while switching and limits the charging current while slowing
162 the charging time to avoid sparking. After discharge damage that prevented
163 applying the full voltage, this resistor was changed to $200\text{ M}\Omega$ to compensate
164 for the leakage. The vertical $1\text{ k}\Omega$ resistor limits transient currents to the ad-
165 missible rating of the switch (150 A). **Finally, a $120\text{ }\Omega$ resistor (left) matches**
166 **the switch impedance and stray capacitance to the load.** We obtained a
167 risetime of roughly 200 ns .

168 Each electrode lens of the decelerator is connected to a separate power
169 supply, which is controlled via a LabVIEW[®] program and a National Instru-
170 ments compact-DAQ interface. An essential step before using the decelerator
171 is the high-voltage conditioning of each electrode. When applying over 10

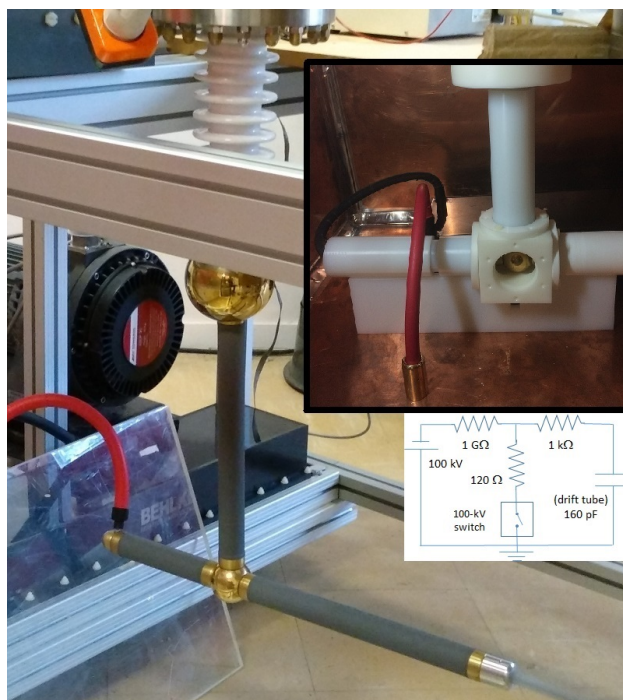


Figure 4: Photograph of the switching circuit, high-voltage connections, resistors (grey) and switch (black). Connection to the 100 kV supply is on the right. Inset photograph shows the resistors with their teflon cladding, installed in a copper Faraday cage. Lower inset shows the circuit diagram (values discussed in the text).

172 kV to an electrode, contamination on the surfaces provokes small discharges
 173 which cause spikes in vacuum pressure. The high-voltage conditioning actu-
 174 ally cleans and helps outgas the surfaces but must not be rushed since an arc
 175 easily leaves a trace that can be impossible to burn away. After mounting
 176 and baking the chambers, this process took several hours for each electrode
 177 to reach its required voltage.

178 A photograph of the decelerator system vacuum chambers connected to
 179 the ELENA beamline is shown in Fig. 5. A 300 l/s ion pump is mounted

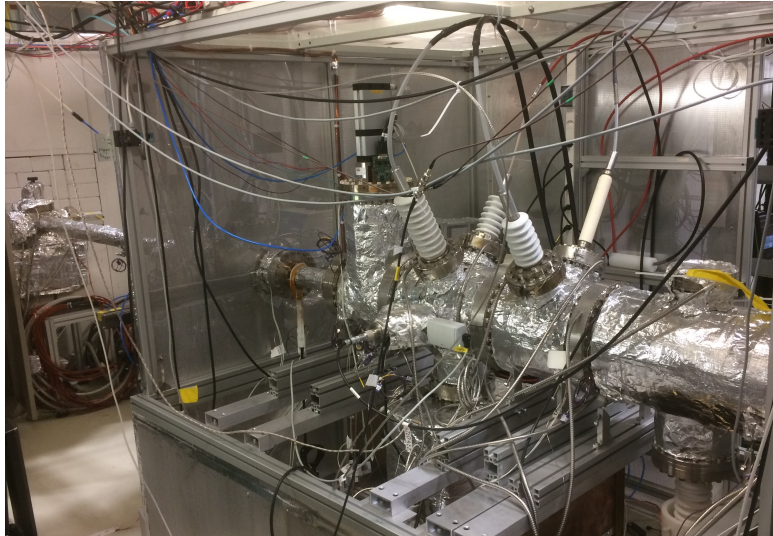


Figure 5: Photograph of the installed decelerator system and high-voltage connections (see technical drawing in Fig. 2). The 100 kV Behlke switch is located below the system. The beamline connected to the ELENA extraction line (LNE50) is visible on the left side, as is the white wall separating the GBAR and ELENA zones. The high-voltage protection cage is also visible (the foreground panel was removed for the photograph).

180 under the first set of deceleration electrodes and a vacuum of 1×10^{-9} mbar
181 was achieved after baking to about 200 degrees Celsius. (Note that neither
182 pump nor port are shown in Fig. 2.)

183 **3. Commissioning tests**

184 The decelerator system was first tested off-line with a 50 keV proton
185 beam, provided by a Penning discharge source and hydrogen-gas leak. A
186 description of the test bench with results from time-of-flight and energy-
187 dispersion tests were reported in [22, 23]. First tests at CERN were carried
188 out using a H^- plasma source connected to ELENA. The H^- beam was in-

189 jected into the ring at 85 keV (sparking in the isolation transformer prevented
 190 higher beam energy). After several turns in the ring, the beam was kicked
 191 into the LNE50 extraction beamline to the decelerator, with its electrodes
 192 grounded. A combination of possible beam optics and diagnostic alignment
 193 problems seems to have prevented the LNE50 quadrupoles from focusing the
 194 beam through the first apertures of the decelerator line. As a result, we
 195 were not able to transport the beam to the decelerator with the calculated
 196 nominal optical element values.

197 We also performed tests with antiproton bunches decelerated from 5.3
 198 MeV by the ELENA storage ring and delivered at 100 keV. While the AD
 199 cycle for antiprotons is much slower (one pulse every 110 s, compared to
 200 about every 5 s using the H^- source) the antiproton annihilation detected
 201 by scintillators along the beamline provides an excellent diagnostic for beam
 202 losses.

203 The deceleration of ELENA antiprotons is illustrated by the following dis-
 204 cussion and figures. First, Fig. 6 illustrates the GBAR beam-line elements,
 205 detectors and relative distances after the handover point at the end of the
 LNE50 beamline (the wall can be seen in the photograph of Fig. 5). The po-



Figure 6: Schematic view of the decelerator optical elements, PbW_0_4 scintillator detectors and the MCP detector (lenses and drift tube are as in Figure 1). The distance from the end of the drift tube to the MCP is 1170 mm and from the upstream scintillator to the MCP is 700 mm.

206 sition marked “p-Quadrupole” in Fig. 6 is a 12 mm horizontal collimation of
207 an electrostatic quadrupole bender used to steer protons in from a 90-degree
208 angle. During beam tuning with the MCP imaging detector, the shadow of
209 this collimator was clearly visible. With antiprotons an additional scintillator
210 (not shown in the figure) recorded a relatively large annihilation signal, the
211 time of which corresponded to the time of flight of the 100 keV antiprotons
212 from the ELENA deflector. We estimated the resulting transmission to be
213 about 25%.

214 As the tests were performed in parallel with the commissioning of the
215 ELENA machine, it was not possible to perform systematic studies. A critical
216 parameter for successful deceleration of the beam pulse is the timing of the
217 drift-tube switch with respect to the ELENA extraction (an electrostatic
218 septum that is switched from ground to a given extraction voltage). This
219 pulse was fed into a digital delay generator to generate the trigger for the
220 switch.

221 Fig. 7 shows screen shots of the scintillator and MCP detector oscilloscope
222 traces and MCP antiproton-beam images (inset). The top panel was recorded
223 with the trigger too early and the bottom panel with the trigger too late.
224 An early trigger means that the drift tube is pulsed to ground before the
225 antiproton pulse arrives. Therefore the antiprotons see no potential on the
226 drift tube and experience no deceleration. The late trigger causes the drift
227 tube voltage to remain at its set value (here it was -90 kV) during the transit
228 of the antiproton pulse. This results in an initial deceleration of the pulse and
229 reacceleration to 90 keV after transiting the drift tube at 10 keV. (There were
230 no voltages on the other electrodes for this measurement.) The difference in

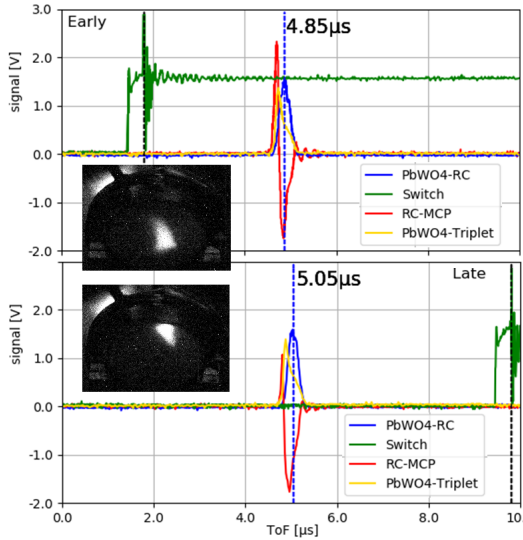


Figure 7: Static voltage operation showing detector-signal oscilloscope traces: HV-switch trigger (green - the black dotted line is the true switching time, visible from the high-amplitude noise); a PbWO_4 crystal located above the quadrupole triplet (yellow); a PbWO_4 crystal located above the MCP (blue); the MCP signal (red). The top panel corresponds to an early trigger (no deceleration) and the bottom to a late trigger (90 keV deceleration and subsequent reacceleration to ground exiting the drift tube). The 200 ns ToF difference between the full-energy and slowed/re-accelerated beam annihilation signals is indicated. Insets show antiproton-beam images recorded by a CCD camera facing upwards to the inclined MCP detector.

231 time of flight between the full-energy beam and slowed/re-accelerated beam
 232 is calculated to be about 200 ns, which is visible from the oscilloscope traces.

233 The scintillator signals in Fig. 7 show a time difference of roughly 150
 234 ns between annihilation of antiprotons hitting the upstream triplet and the
 235 downstream MCP. This corresponds quite well to the calculated time of flight
 236 of 160 ns for 100 keV antiprotons over the 700 mm separating the detectors.

237 The (inset) MCP images in Fig. 7 show the beam to be relatively well

238 centered, but when decelerated by the drift tube a vertical shift of about 15
 239 mm is visible (the MCP diameter is 42 mm, inclined by 45 degrees). The
 240 beam is somewhat focused by the drift tube since it forms a long Einzel lens.
 241 Because of the possible alignment problems (mentioned at the beginning of
 242 this section) it seems plausible that the beam was not injected along the
 243 decelerator drift-tube axis, which could explain the movement of the beam
 244 under deceleration.

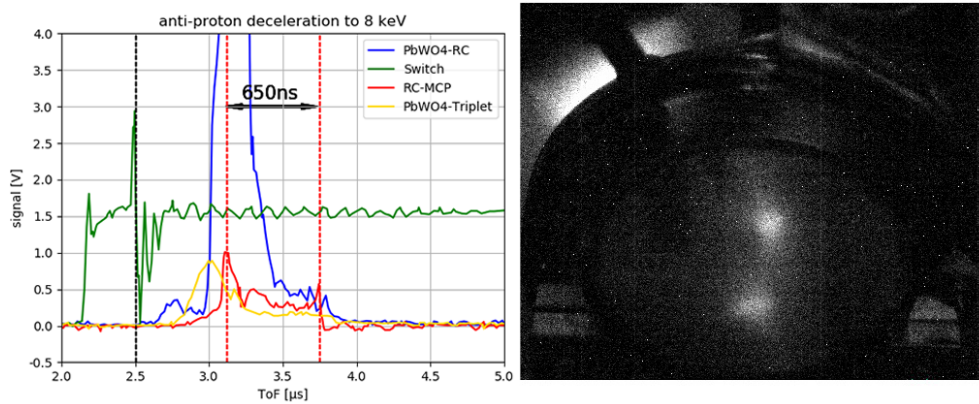


Figure 8: Demonstration of antiproton deceleration from 100 to 8 keV. As in Fig. 7 the right image was recorded by a CCD camera facing the MCP. The left panel shows recorded oscilloscope traces: Behlke-switch trigger (green); PbWO_4 crystal located above the upstream lenses (yellow); PbWO_4 crystal located above the MCP (blue), and MCP signal (red). The trigger was set to switch the drift-tube voltage while the pulse was inside. The MCP trace shows both the 8 keV decelerated component (later peak) and part of the undecelerated 100 keV beam (earlier peak). The CCD image (right) shows these two components that are spatially distinct, as seen separately in Fig. 7.

245 Because of the discharge on the drift tube mentioned earlier, we were only
 246 able to apply -92 kV before the maximum rated current of the supply was
 247 reached. The lowest achievable beam energy was therefore only 8 keV.

248 In the meantime, we have learned that the drift tube insulator assembly
249 may be insufficiently shielded, forming a so-called triple junction effect at
250 the insulator/conductor interface [28]. This would explain not only the dis-
251 charge but also the deflection of the decelerated beam, due to charging on
252 the insulator. The “cradle” is therefore being redesigned.

253 Fig. 8 illustrates the deceleration of the 100 keV ELENA beam to 8 keV
254 under the aforementioned conditions. On the right side of the figure, the
255 CCD camera image of the MCP shows two distinct beam spots. We believe
256 the upper spot corresponds to the decelerated fraction of the beam pulse and
257 the lower spot corresponds to a “fast” (non-decelerated) fraction. This is
258 corroborated by the static test shown in Fig. 7 where the beams are not seen
259 at the same position because of the early and late triggering. The alignment
260 problem mentioned earlier leads to shifts in beam position and angle which
261 are amplified by the deceleration process. This effect has been reproduced
262 by simulations.

263 But while the static test might imply the that the lower spot corresponds
264 to the decelerated antiprotons, we discovered in subsequent tests that the
265 triple-junction effect explained by Faircloth [28] can also charge the insulator
266 and slightly deflect the decelerated beam downward. Since the injection
267 conditions were not the same as for the static case, it is not possible to say
268 with absolute certainty.

269 The MCP signal (red trace in Fig. 8) shows two maxima with a time
270 difference of about 650 ns, corresponding to two groups of antiprotons: one
271 “fast” (non-decelerated) group and one “decelerated” group. As mentioned,
272 the reaction chamber MCP is 1170 mm downstream of the drift tube. The

273 calculated time-of-flight difference for antiprotons at 100 and 8 keV over this
274 distance is 675 ns, in good agreement with the detected MCP pulses shown
275 in Fig. 8 (although the timing resolution is rather limited). There is also a
276 continuum between the two peaks caused by antiprotons that experience the
277 fringe field at the exit of the drift tube, convoluted with the 200 ns switching
278 time. We believe this happens because the ELENA pulse length was likely
279 longer than the 300 ns design value so that the entire pulse could not fit
280 inside the drift tube before switching.

281 From integrating the areas under the peaks (assuming identical MCP
282 signal response for 100 keV and 8 keV antiprotons) we find the decelerated
283 fraction is about 25% compared to the fast antiprotons. Because of the
284 compressed commissioning schedule of ELENA, it was not possible to test
285 different optical configurations for the decelerating lenses.

286 To explore the continuum effect visible in Fig. 8, ion trajectory calcula-
287 tions were performed to simulate the MCP signal, with the results shown in
288 Fig. 9. As during the experimental tests, -92 kV was applied to the drift
289 tube with the other decelerating lenses at ground. The three panels show
290 different input pulse durations of 10, 400 and 600 ns (the design value is
291 300 ns [15]). The switching pulses were modeled using an exponential decay,
292 with the measured time constant of 200 ns. The switch is always triggered
293 while the beam is centered in the drift tube. For the hypothetical case of
294 10 ns (top panel), a single decelerated pulse is seen, as expected. The in-
295 creased width of the peak is due to the large (125 eV) energy spread quoted
296 in the ELENA design [15]. When the beam occupies the areas near the
297 drift-tube edges (middle panel), the antiprotons experience varying amounts

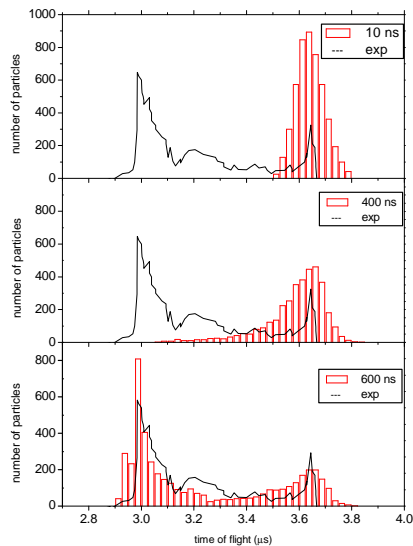


Figure 9: Simulated time-of-flight histograms (red columns) of antiprotons decelerated from 100 keV to 8 keV with different injected pulse durations. Top panel shows a beam pulse of only 10 ns for reference. The middle panel shows a 400 ns pulse that results in a decelerated pulse of 497 mm in length, which clearly does not fit into the drift tube. The bottom panel shows a 600 ns pulse that produces decelerated and re-accelerated beam components. The recorded MCP pulse is also shown (solid back line).

298 of re-acceleration and “leak out” of the main peak to earlier arrival times.
 299 With the pulse protruding even farther out of both ends of the drift tube
 300 (bottom panel), the continuum seen in the measurements (Fig. 8, left panel)
 301 appears. The recorded MCP signal (slightly shifted in time and scaled in
 302 amplitude) is also included in the figure for comparison.

303 The simulations showing the 100 keV and 8 keV antiproton-deceleration
 304 peaks agree with the measured 650 ns time-of-flight difference to within about

305 25 ns, or better than 4%. The ELENA pulse length was not monitored dur-
306 ing the tests. A CERN internal note concerning low-level RF tests during
307 the ELENA commissioning reports a typical pulse of 600 ns that was im-
308 proved at one stage to 200 ns (see Fig. 34 in [29]). The 600 ns pulse length
309 qualitatively matches our measurements. The simulated peaks have larger
310 widths compared to the measurement, which may indicate that the projected
311 ELENA energy spread of 0.125% is too conservative.

312 In a final test, the decelerated antiprotons were transported 2 m down-
313 stream of the reaction chamber, through a beam switchyard designed to
314 separate unreacted antiprotons from neutral antihydrogen and the antihy-
315 drogen ions (see chapter 6 of [23]). An antiproton signal was detected with
316 an MCP mounted on the straight section and could be moved laterally by
317 applying the switchyard-electrode voltages (see sections 7.5 and 8.5 of [30]).
318 Again, due to experimental restrictions, we could not obtain quantitative
319 information.

320 4. Summary

321 We have presented a new scheme using electrostatic optics and fast high-
322 voltage switching for decelerating antiproton bunches down to keV energies
323 for precision experiments such as GBAR at the CERN AD facility. Such a
324 scheme avoids losses associated with passing the beam through thin foils, and
325 should offer increased efficiency. A detailed technical description of the decel-
326 erator design and realization has been given. Prior to CERN's second Long
327 Shutdown (LS2) we successfully commissioned the first 100 keV pulsed drift
328 tube and electrostatic-lens system built to decelerate the pulsed antiproton

329 beam from the ELENA storage ring of CERN’s AD “antimatter factory”.
330 Because the tests were performed during the very short commissioning of
331 ELENA, only limited results could be obtained. Our results give clear ev-
332 idence of antiproton pulses decelerated to 8 keV. Since the ELENA pulses
333 were longer than the design value of 300 ns, only a fraction of the antiprotons
334 were decelerated. This situation will be improved when CERN restarts in
335 mid-2021.

336 5. Acknowledgements

337 We thank J. Bui, S. Cabaret, P. Dupré, P. Duarte, S. Hervé, D. Le Du,
338 H. Lefort, A. Limongi, V. Manea, S. Martineau, K. Nguyen, S. Pitrel and H.
339 Ramirijaona from the CSNSM, C. Doré from the LKB, J.-L. Babigeon from
340 the LAL, D. Desforges, Ph. Hardy, S. Javello, D. Pierrepont and C. Vuillemin
341 from the CEA and F. Butin from CERN for their various contributions. We
342 warmly thank the ELENA team for their help and cooperation during the
343 tests.

344 The decelerator project was supported by France’s IN2P3, by the *Agence*
345 *Nationale de Recherche* under project no. ANR-14-CE33-0008 (ANTION),
346 and by the *Laboratoire d’Excellence* P2IO (ANR-10-LABX-0038) in the frame-
347 work *Investissements d’Avenir* (ANR-11-IDEX-0003-01).

348 6. References

- 349 [1] P. Pérez, et al., The gbar antimatter gravity experiment, *Hyperfine*
350 interactions 233 (2015) 21–27.

- 351 [2] C. Amole, et al., Description and first application of a new technique
352 to measure the gravitational mass of antihydrogen, *Nature Communi-*
353 *cations* 4 (2013) 1785.
- 354 [3] S. Aghion, et al., A moiré deflectometer for antimatter, *Nature Com-*
355 *munications* 5 (2014) 4538.
- 356 [4] C. Monroe, D. Meekhof, B. King, S. R. Jefferts, W. M. Itano, D. J.
357 Wineland, P. Gould, Resolved-sideband raman cooling of a bound atom
358 to the 3d zero-point energy, *Physical Review Letters* 75 (1995) 4011.
- 359 [5] L. Hilico, J.-P. Karr, A. Douillet, P. Indelicato, S. Wolf,
360 F. Schmidt Kaler, Preparing single ultra-cold antihydrogen atoms for
361 free-fall in gbar, in: *International Journal of Modern Physics: Confer-*
362 *ence Series*, volume 30, World Scientific, p. 1460269.
- 363 [6] N. Sillitoe, J.-P. Karr, J. Heinrich, T. Louvradoux, A. Douillet, L. Hilico,
364 Sympathetic cooling simulations with a variable time step, in: *Proceed-*
365 *ings of the 12th International Conference on Low Energy Antiproton*
366 *Physics (LEAP2016)*, p. 011014.
- 367 [7] L. Liskay, M.-F. Barthe, C. Corbel, P. Crivelli, P. Desgardin, M. Eti-
368 enne, T. Ohdaira, P. Pérez, R. Suzuki, V. Valtchev, A. Walcarius, Or-
369 thopositronium annihilation and emission in mesostructured thin silica
370 and silicalite-1 films, *Applied Surface Science* 255 (2008) 187.
- 371 [8] L. Liskay, with the GBAR Collaboration, *Nucl. Instrum. Meth. A* 985
372 (2021) 164657.

- 373 [9] S. Niang, et al., Accumulation of positrons from a linac based source.,
374 Acta Physica Polonica, A. 137 (2020) 164.
- 375 [10] J. Humberston, M. Charlton, F. Jacobsen, B. Deutch, On antihydrogen
376 formation in collisions of antiprotons with positronium, J. Phys. B: At.
377 Mol. Phys. 20 (1987) L25.
- 378 [11] J. P. Merrison, H. Bluhme, J. Chevallier, B. I. Deutch, P. Hvelplund,
379 L. V. Jorgensen, H. Knudsen, M. R. Poulsen, M. Charlton, Hydrogen
380 formation by proton impact on positronium, Phys. Rev. Lett. 78 (1997)
381 2728.
- 382 [12] P. Comini, P.-A. Hervieux, \bar{H}^+ ion production from collisions between
383 antiprotons and excited positronium: cross sections calculations in the
384 framework of the GBAR experiment, New Journal of Physics 15 (2013)
385 095022.
- 386 [13] A. S. Kadyrov, C. M. Rawlins, A. T. Stelbovics, I. Bray, M. Charlton,
387 Antihydrogen formation via antiproton scattering with excited positro-
388 nium, Phys. Rev. Lett. 114 (2015) 183201.
- 389 [14] T. Yamashita, Y. Kino, E. Hiyama, K. Piszczatowski, S. Jonsell,
390 P. Froelich, Towards prediction of the rates of antihydrogen positive
391 ion production in collision of antihydrogen with excited positronium,
392 Journal of Physics: Conference Series 1412 (2020) 052012.
- 393 [15] W. Bartmann, P. Belochitskii, H. Breuker, F. Butin, C. Carli, T. Eriks-
394 son, W. Oelert, R. Ostojic, S. Pasinelli, G. Tranquille, The ELENA
395 facility, Phil. Trans. R. Soc. A 376 (2017) 20170266.

- 396 [16] G. Gabrielse, X. Fei, K. Helmerston, S. L. Rolston, R. Tjoelker, T. A.
397 Trainor, H. Kalinowsky, J. Haas, W. Kells, First capture of antiprotons
398 in a penning trap: A kiloelectronvolt source, *Phys. Rev. Lett.* 57 (1986)
399 2504–2507.
- 400 [17] G. Gabrielse, N. Bowden, P. Oxley, A. Speck, C. Storry, J. Tan, M. Wes-
401 sels, D. Grzonka, W. Oelert, G. Schepers, T. Sefzick, J. Walz, H. Pittner,
402 T. Haensch, E. Hessels, Stacking of cold antiprotons, *Physics Letters B*
403 548 (2002) 140 – 145.
- 404 [18] M. Hori, The asacusa experiment at cern’s antiproton decelerator, *Nucl.*
405 *Phys. A* 692 (2001) 119 – 128.
- 406 [19] N. Kuroda, H. A. Torii, K. Y. Franzen, Z. Wang, S. Yoneda, M. Inoue,
407 M. Hori, B. Juhász, D. Horváth, H. Higaki, A. Mohri, J. Eades, K. Ko-
408 maki, Y. Yamazaki, Confinement of a large number of antiprotons and
409 production of an ultraslow antiproton beam, *Phys. Rev. Lett.* 94 (2005)
410 023401.
- 411 [20] N. Kuroda, H. A. Torii, Y. Nagata, M. Shibata, Y. Enomoto, H. Imao,
412 Y. Kanai, M. Hori, H. Saitoh, H. Higaki, A. Mohri, K. Fujii, C. H.
413 Kim, Y. Matsuda, K. Michishio, Y. Nagashima, M. Ohtsuka, K. Tanaka,
414 Y. Yamazaki, Development of a monoenergetic ultraslow antiproton
415 beam source for high-precision investigation, *Phys. Rev. ST Accel.*
416 *Beams* 15 (2012) 024702.
- 417 [21] D. Lunney, P. Dupré, P. Grandemange, V. Manea, T. Mortensen,
418 S. Cabaret, S. Pitrel, P. Comini, P. Debu, L. Liskay, P. Lotrus, P. Pérez,

- 419 J.-M. Rey, J.-M. Reymond, N. Ruiz, Y. Sacquin, B. Vallage, D. Brook-
420 Roberge, P. Hardy, *Hyp. Interact.* 229 (2014) 1.
- 421 [22] A. Husson, D. Lunney, arXiv:1909.07493 (2016).
- 422 [23] A. Husson, Deceleration of antiprotons from cern's elena syn-
423 chrotron and transport of antimatter beams through the gbar
424 experiment, Doctoral Thesis, Université Paris-Saclay (2018)
425 <http://cds.cern.ch/record/2712543>.
- 426 [24] F. Herfurth, J. Dilling, A. Kellerbauer, G. Bollen, S. Henry, H.-J. Kluge,
427 E. Lamour, D. Lunney, R. B. Moore, S. Scheidenberger, S. Schwarz,
428 G. Sikler, J. Szerypo, *Nucl. Instrum. Meth. A* 469 (2001) 254.
- 429 [25] S. Coeck, B. Delaur, M. Herbane, M. Beck, V. Golovko, S. Kopecky,
430 V. Kozlov, I. Kraev, A. Lindroth, T. Phalet, D. Beck, P. Delahaye,
431 A. Herlert, F. Wenander, N. Severijns, A pulsed drift cavity to cap-
432 ture 30keV ion bunches at ground potential, *Nuclear Instruments and*
433 *Methods in Physics Research Section A: Accelerators, Spectrometers,*
434 *Detectors and Associated Equipment* 572 (2007) 585 – 595.
- 435 [26] J. Grund, M. Asai, K. Blaum, M. Block, S. Chenmarev, C. Dllmann,
436 K. Eberhardt, S. Lohse, Y. Nagame, S. Nagy, P. Naubereit, J. van
437 de Laar, F. Schneider, T. Sato, N. Sato, D. Simonovski, K. Tsukada,
438 K. Wendt, First online operation of triga-trap, *Nuclear Instruments*
439 *and Methods in Physics Research Section A: Accelerators, Spectrome-*
440 *ters, Detectors and Associated Equipment* 972 (2020) 164013.

- 441 [27] C. Smorra, High-precision q-value and mass measurements for neutrino
442 physics with triga-trap and commissioning of an on-line ion source for
443 triga-spec, Ph.D. thesis, University of Heidelberg (2012).
- 444 [28] D. C. Faircloth, Technological Aspects: High Voltage, in CAS - CERN
445 Accelerator School: Ion Sources 10.5170/CERN-2013-007.381 (2013)
446 381–419, <https://cds.cern.ch/record/2703432>.
- 447 [29] M. E. Angoletta, M. Jaussi, J. Molendijk, New llrf capabilities and
448 beam results for the second year of elenas commissioning, CERN-ACC-
449 NOTE-2019-0050 (2019) <https://cds.cern.ch/record/2703432>.
- 450 [30] B. Latacz, Study of the antihydrogen atom and ion produc-
451 tion via charge exchange reaction on positronium, Doctoral The-
452 sis, Université Paris-Saclay (2019) [https://tel.archives-ouvertes.fr/tel-](https://tel.archives-ouvertes.fr/tel-02417434/document)
453 [02417434/document](https://tel.archives-ouvertes.fr/tel-02417434/document).